2018-03-01

Confocal Raman Spectroscopic Imaging for In Vitro Monitoring of Active Ingredient Penetration and Distribution in Reconstructed Human Epidermis Model

Lynda Miloudi
Université François-Rabelais de Tours, faculty of pharmacy, EA6295 Nanomédicaments et Nanosondes, Tours, France

Franck Bonnier
Universite Francois-Rabelais de Tours,faculty of pharmacy, EA6295 Nanomédicaments et Nanosondes, Tours, France.

Ali Tfayli
EA7357 Lip (Sys)2 "Lipides : Systèmes Analytiques et Biologiques", Faculty of Pharmacy, University Paris Saclay, Châtenay-Malabry, France

See next page for additional authors

Recommended Citation
Miloudi, L., et al. (2018). Confocal Raman Spectroscopic Imaging for In Vitro Monitoring of Active Ingredient Penetration and Distribution in Reconstructed Human Epidermis Model. *Journal of Biophotonics*, vol. 11, no. 4, e201700221. doi: 10.1002/jbio.201700221

Confocal Raman spectroscopic imaging for in vitro monitoring of active ingredient penetration and distribution in Reconstructed Human Epidermis model

Lynda Miloudi[1], Franck Bonnier[1], Ali Tfayli[2], Florent Yvergnaux[3], Hugh J. Byrne[4], Igor Chourpa[1] and Emilie Munnier[1]*

[1] Université François-Rabelais de Tours, Faculty of Pharmacy, EA6295 Nanomédicament et Nanosondes, 31 avenue Monge, 37200 Tours, France
[2] EA7357 Lip (Sys)2"Lipides : Systèmes Analytiques et Biologiques", Faculty of Pharmacy, University Paris Saclay, Chatenay-Malabry, France
[3] Bioeurope Solabia Group, Anet, France
[4] FOCAS Research Institute, Dublin Institute of Technology, Kevin Street, Dublin 8, Ireland

Key words: Confocal Raman micro-spectroscopy, Human Reconstructed Epidermis (RHE), Delipidol®, K-means clustering analysis, NCLS, penetration profiles.

Topically applied Active Cosmetic Ingredients (ACI) or Active Pharmaceutical Ingredients (API) efficacy is directly related to their efficiency of penetration in the skin. In vitro Reconstructed Human Epidermis (RHE) surrogate models offer in vivo like skin samples for transdermal studies. Using Delipidol®, an ACI currently used in the cosmetics industry, the capabilities to deliver accurate distribution maps and penetration profiles of this molecule by means of Confocal Raman spectroscopic Imaging have been demonstrated. Using a NCLS (Non negative constrained least squares) approach, contribution of specific molecules can be estimated at each point of spectral maps in order to deliver semi-quantitative heat maps representing the ACI levels in the different skin layers. The concentration profiles obtained are approximately single exponential for all three time points evaluated, with a consistent decay constant, which is independent of the sublayer structure. Notably, however, there is no significant penetration into the lower basal layers until a critical concentration is built up, after 3 hours. Combination of Raman Confocal Imaging with spectral unmixing methods such as NCLS is demonstrated to be a relevant approach for in vitro biological evaluation of cosmetic and pharmaceutical active ingredients and could easily be implemented as screening tool for industrial use.

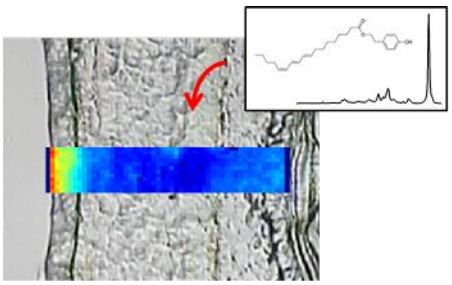

1. Introduction

Topical applications, i.e. directly on the skin surface, of pharmaceutical and cosmetic formations are systematically confronted by the strong barrier function of the *stratum corneum*. The first shield against intrusion of exogenous agents, the outer layer of the skin generally presents low permeability to Active Cosmetic Ingredients (ACI) and Active Pharmaceutical Ingredient (API). Therefore, penetration and diffusion assays of newly designed molecules for skin care or medical purposes need to be conducted to ensure maximum efficacy can be reached. The general procedure for assessing the penetration and diffusion of a molecule into the human skin is performed by several techniques such as diffusion cells coupled with HPLC (High Performance Liquid Chromatography) [1] or tape stripping [2]. However, important information regarding the lateral spatial distribution or accumulation effects in skin layers cannot be assessed. Another analytical method based on radiolabelling is used into the field of drug delivery [3], but it is not widely used due to the complexity of the method and hence it is not suitable for routine screening. Techniques like electron microscopy (EM) [4], small angle X-Ray scattering techniques (SAXS) [5], confocal laser scanning microscopy (CLSM) [6, 7] and multiphoton microscopy (MPM) [8] are extensively used for tissue imaging, but are either dependent on the use of fluorescent probes or only deliver histological information and therefore cannot detect and track an exogenous chemical agent. Vibrational spectroscopy is a mean of establishing a fingerprint of a material through the characteristic molecular vibrations. It is a routine technique for fingerprinting and identifying chemicals and acts as a standard method of analytical pharmacy and chemistry [9]. Raman spectroscopy has been demonstrated to have higher spatial and spectral resolution than IR spectroscopy bench top instruments, potentially providing subtle information of the molecular composition and organization of the tissue [10]. Moreover, following developments achieved in recent years, numerous experimental challenges associated with the measurement of chemical and physical inhomogeneity can be surmounted [11, 12], further strengthening the Raman capability for skin analysis. Its potential for dermatological application has been demonstrated [13], whereby the spectral information can be used to assess the chemical integrity of the skin [14], the hydration state [15], oxidative stress and the ability to individually track various ingredients of a formulation [16]. It has also been widely used for monitoring active molecules in the skin [13, 17–21]. It can provide valuable information on the lateral distribution, kinetics, rate and depth of penetration of these molecules in skin layers without the use of probe molecules [21]. The improvements made in the data handling procedures through the implementation of multivariate analysis has considerably increased the relevancy of the information contained in the spectral data [22]. Multivariate statistical methods such as K-means clustering and Principal Components analysis are routinely used for analysis of spectral images [22, 23] and have been proven to be powerful tools for rapid analysis and stratification of tissue sections to identify the presence of pathologically relevant areas [24]. However, such methods can be limited when working on a complex multilayered tissue such as the skin, with no clinical abnormalities *per se* (lesions, tumors) but only variations in the chemical compositions through the different layers either resulting from physiological mechanisms or the diffusion of exogenous molecules. Recent changes in European Union directives (2010/63/EA) encourage the use of artificial and reconstructed skin models as alternatives to *in vivo* and *ex vivo* testing of transdermal delivery of pharmacological or cosmetic products [11]. This approach offers the possibility to carry out several replicate measurements with a convenient reproducibility of the results while avoiding ethical problems [25]. It has been demonstrated that the different *in vitro* skin models exhibit reasonable similarities to the native human skin in terms of morphology, lipid composition and biochemical markers [26, 27]. In the present study, the capabilities of confocal Raman imaging for monitoring of active ingredients has been evaluated using the Episkin® Reconstructed Human Epidermis (RHE) model, offering a dermal equivalent, constituted by a differentiated epidermis derived from normal human keratinocytes cultured on a collagen matrix at the air-liquid interface, offering a model histologically similar to the *in vivo* human epidermis. Such a model is perfectly suited for penetration studies [28] but also represents one of most widely used models in the cosmetics industry. While recent advancements have supported the feasibility to perform Z profiling with step by step data collection from the skin sample surface [25, 29], methodologies need to be in accordance with potential user expectations. Without trying to compare the benefits of whole sample versus thin sections, a simple fact remains that colour coded distribution maps of an ACI remain one of strongest and most convincing representation for industries and their customers to prove their product penetrates efficiently. In this context, Delipidol® (BioEurope Solabia, France) has been selected as a test molecule to develop and optimise data mining approaches to rapidly and accurately chemical map the skin model to evaluate its kinetics of penetration by means of Non negative constrained least squares (NCLS) analysis. Although primarily used previously in the digital dewaxing of Raman and Infrared spectra recorded from partially chemically dewaxed tissue samples [30] and background subtraction [31], the

method is an attractive data analytical option, delivering abundance fraction (concentration) estimation of chemical and biological agents that exist in the mixture form [32]. Ultimately, distribution maps and penetration profiles can be obtained from the Raman datasets, providing crucial information about the ACI diffusion and distribution in the skin, consequently supporting the translation of Raman Confocal Imaging to industrial application for screening and identification of the next relevant candidates for cosmetic product development and optimization.

2. Materials and Methods

2.1 Reagents

Biochemical compounds used as reference material (ceramide, cholesterol, phosphatidylcholine (PDC), stearic acid, albumin, histone, DNA) were purchased from Sigma-Aldrich (France). Delipidol®, the ACI evaluated in the present study, was provided by BioEurope (Solabia group, France) under a scientific partnership aiming to developed new tools for biological evaluations linked to the cosmetics industry. Delipidol® is a hydrophobic anti-cellulite molecule, and a 10% solution (m/v) was prepared by dissolving 1g in 10 mL of ethanol. The concentration of 10% Delipidol® has been selected in order to match with the composition of commercialized cosmetic products as recommended by BioEurope (Solabia group, France). While the ethanol is a solvent acting as penetration enhancer, it is expected full evaporation will be observed during the preparation of thin sections leading to no possible spectral interferences during analysis. The use of 10g/L solution ensures that if Delipidol® diffuses through the *stratum corneum* the concentrations observed would be sufficiently high for detection with Raman spectroscopy. Moreover, the presence of particularly strong features in the ACI signature further inverse the sensitivity of the method for its detection. Ceramide, PDC, Cholesterol, and stearic acid, were first dispersed in chloroform while solutions of albumin, histone and ADN were prepared in distilled water before deposition of small amounts of material onto CaF_2 substrates followed by air drying before Raman spectra acquisitions.

2.2 Preparation of Tissue samples

Reconstructed Human Epidermis (RHE) inserts were purchased from Episkin® (Lyon, France). Episkin® RHE are human like epidermis inserts (1.07 cm^2) consisting of a stratified and fully differentiated epidermis derived from human keratinocytes laying on a type I collagen matrix, representing the dermis, surfaced with a film of type IV collagen [33]. The RHE inserts are presented in 12 well plates with maintenance medium (about 2 mL) added to each well before incubation (5% CO_2, 37°C, 95% humidity). This model can be used at different stages of maturity, for instance the present work has been conducted skin samples cultured for 14 days. Prior to topical application (i.e. exposure to ACI) the RHE units were placed at room temperature for 30 min. 200 µL of the Delipidol® solution (prepared as described in section 2.1) were applied directly on the surface of each insert followed by incubation times of 1h, 2h or 3h. The Delipidol® being used in commercialized products at concentrations up to 10% without warning about possible toxicity, it has been considered the innocuousness and efficacy of the active ingredients were tested by the supplier and therefore not discussed throughout this study. Only the capabilities to detect the ACI by means of Raman imaging coupled to multivariate analysis have been explored. At the end of the exposure time, the remaining Delipidol® solution was taken off and a quick wash with ethanol was done to ensure no residual traces of the stock solution could be found on the skin surface. Additionally, untreated skin inserts have also been prepared in parallel as blank control samples. For Raman analysis, 20 µm thin sections have been prepared using a cryo-microtome (Leica CM 1850 UV) and were deposited on CaF_2 Raman grade substrates (Crystran, UK). The samples were stored at -20°C until data collection. All samples have been prepared in triplicates (n=3) and subjected to Raman confocal imaging. The RHE enable high reproducibility with no variation in the results observed between replicates. Therefore, it has been decided to rather put emphases on the NCLS itself with one Raman map to selected as an illustration for each condition tested.

2.3 Raman spectroscopy

Raman spectra were acquired using a LabRam (Horiba Jobin-Yvon, France). Raman scattering was obtained using a 691 nm diode laser with a power of 8 mW at the sample, under a x50 objective LMPlan (Olympus, NA 0.75). The confocal hole was set at 250 µm for all measurements. The system was spectrally calibrated to the 520.7 cm^{-1} spectral line of silicon each day. Detection was facilitated by dispersing Raman-shifted radiation onto a CCD detector using a grating (300 lines/mm). For consistency, in this manuscript, all spectral images of the Episkin® RHE sections are displayed with the *Stratum corneum* oriented to the left. The laser spot size is estimated to be below 2 µm with acquisition parameters

used, therefore the step sizes used were 2 µm in the X direction and 3 µm for the Y in order to avoid oversampling during mapping. An acquisition time of 2 x 15s per spectrum was employed, over the 400-1800 cm^{-1} spectral range. The acquisition of 2D images has been preferred in the present study in order to capture both depth penetration and possible lateral variability that can be observed in case of heterogeneous diffusion of the ACI. The purpose of the study being to illustrate the capabilities of the NCLS analysis, the analysis has been limited to areas of roughly 20 * 180 $µm^2$ but the method could be indeed applied to much larger Raman maps.

2.4 Data handling

Data analysis was performed using Matlab (Mathworks, USA). Before statistical analysis, Raman spectra were subjected to linear baseline correction (in house rubber band with only 2 nodes) [34] then vector normalised. In line with previous analyses of human skin tissue sections [11], K-means clustering analysis was then used to analyze the spectral variation in spectral image of the tissue sections [35]. It groups the spectra according to their similarity, forming clusters, each one representing regions of the image with identical molecular properties. The distribution of chemical similarity can then be visualized across the sample spectral image. The number of clusters (k) has to be determined a priori by the operator before initiation of the classification of the data set. K centroids are defined, ideally as far as possible from each other, and then each point belonging to a data set is associated to the nearest centroid. When all the points have been associated with a centroid, the initial grouping is done. The second step consists of the calculation of new centroids as barycentres of the clusters resulting from the previous step. A new grouping is implemented between the same data points and the new centroids. These operations are repeated until convergence is reached and there is no further movement of the centroids. Finally, k clusters are determined, each containing the most similar spectra from the image. Ultimately, colors can be attributed to each cluster and false colors maps can be constructed to visualize the organization of the clusters in the original image.[36]

Principal Component Analysis (PCA) is a multivariate analysis technique that is widely used to simplify a complex data set of multiple dimensions [37]. It allows the reduction of the number of variables in a multidimensional dataset, although it retains most of the variation within the dataset. The other advantage of this method is the derivation of PC loadings which represent the variance of each variable (wavenumber) for a given PC. Analysis of the loading of a PC can give information about the source of the variability inside a dataset, derived from variations in the chemical components contributing to the spectra [38]. In this work, PCA is used to either highlight the biochemical changes between skin layers identified by means of K-means clustering or intra-variability observed in spectra isolated from the *stratum corneum*.

Non-negatively Constrained Least Squares analysis (NCLS) is a powerful method described by Kwan et al [39] for the unmixing of spectral data. The strength of the approach is the estimation of the contribution of each feature in the signal collected from the samples based on a set of references spectra used to perform the fitting. Thus, using spectral signatures obtained from pure biomolecules as references, the concentrations (or abundance fractions) of the physiological skin constituents but also of the ACI can be estimated. Moreover, the originality of this method is to add to a classical least squares procedure, a positivity constraint on concentrations. In summary, the algorithm works on a pixel-to-pixel fashion with each one of them considered as the experimental Raman signature to be reconstituted from the reference spectra set. A simplified description of the NCLS outcome can be defined as:

$$S_S = (S_{R1}.C_1) + (S_{R2}.C_2) + \ldots + (S_{Ri}.C_i) + R$$

Where S_S is the simulated spectrum for a given pixel of the Raman map, S_R are the reference spectra, C the abundance fraction estimated, i the number of reference spectra included in the model and R the residual. The algorithm aims to calculate a S_S has close as possible to the experiential spectrum with minimal residual. More information about the mathematical aspects can be found in references [40]. ”

In the present study, the method is applied to visualize the distribution of the specific compound through Raman spectral images collected from RHE thin sections. Ultimately, the approach enables collection of information about the Delipidol® distribution in both X and Y directions, consequently providing both its penetration profiles at different time points but also to better appreciate the homogeneity of the ACI diffusion (lateral diffusion) across the skin section. Although quantitative capabilities of Raman spectroscopy have been documented for ACI in cosmetic like products models [41], the analysis performed on tissue sections remains to date rather semi-quantitative. The connection between abundance fractions of a given signature in the spectra and actual concentrations remains challenging. For this reason, the NCLS is at present only proposed for evaluation of kinetics of diffusion of Delipidol® and as comparative tool to guide formulation optimization and strategies.

3. Results and discussion

3.1 Reconstructed Human Epidermis (RHE) spectral histology

The human skin is a complex stratified epithelium exhibiting a number of layers which are biochemically different. Most studies of ACI focus mainly on the epidermis which is the outer part of skin. While the basal layers of the epidermis are characterised by the presence of keratinocytes under intense proliferation, the *stratum corneum* is composed of corneocytes (flattened, anuclear cells). The latter results from numerous mechanisms of cellular maturation and differentiation playing a key role in the skin barrier function. The chemical composition, and therefore the spectral signature, significantly differs depending on the depth, thus directly reflecting the changes in cellular morphologies but also in the surrounding matrix (lipids synthesis and reorganization, Natural Moisture Factor accumulation) allowing identification of specific spectral features. Raman spectroscopy can also be affected by other experimental parameters such as the sample thickness/topography leading to substantial variations in intensity but also signal to background ratio [42]. Although thin sections have been prepared using cryo-microtomy, the samples rarely present an even surface throughout the different layers. Nevertheless, performing the data collection with a x50 objective yields consistent and reproducible measurements over the surface, as illustrated in (Figure.S1.A – See supplementary materials), in which raw spectra from the *stratum corneum* are presented. Consequently, applying standard pre-processing methods such as baseline correction (rubber band) and vector normalization is found to be sufficient to remove any undesirable spectral variations prior to data analysis (Figure.S1. B in supplementary materials), resulting in the spectra exhibiting a good signal to noise ratio with the presence of well-defined peaks across the spectral range 400-1800 cm^{-1}.

K-means clustering analysis is a multivariate method widely used to exploit complex data sets contained in hyper-spectral images. The use of such a statistical algorithm allows extraction of the relevant information from the data cubes, highlighting the possible spectral variations connected with biochemical changes in the skin. The method has been proven quite powerful to elucidate tissue histology, in particular for biomedical applications and the identification of pathological areas such as tumors [43, 44]. However, when applied to stratified epithelium such as the skin, the chemical modifications linked to the cellular differentiation mechanism generate heterogeneities in the spectra enabling the creation of clusters according to the different layers of the skin [11] (Figure 1).

Figure 1A shows a bright field image of untreated 20 μm thick tissue section (control sample) as seen on the Raman system with a x50 objective. Without histological staining, the different layers of the skin are rarely visible, although close inspection allows identification of the skin surface (*Stratum corneum*) for orientation of the tissue section and selection of an area of interest for spectral analysis. Following K means clustering, attribution of false colors to the different clusters created (Figure 1B) highlights the stratified biochemical structure of the skin with layers corresponding to the basal layers (cluster 4- green), the *stratum spinosium* (cluster 1- majenta), the *stratum granulosum* (cluster 2- red) and the *stratum corneum* (cluster 3 - blue) clearly defined. The areas corresponding to the CaF2 substrate exhibits poor signal to noise ratio and are consequently identify as part of separate cluster (figure 1B cluster 5). Interestingly, in the model of reconstructed human skin used in the present study, although the layer corresponding to the dermis remains composed of collagen, the sparse organization in the fibers tends to deliver low intensity spectra also included in the cluster 5. Ultimately, all the black pixels in the Kmeans analysis represent irrelevant data points for the subsequent steps of the analysis (i.e. NCLS). However, following the normalization of the spectra corresponding to the substrate, the noise is exacerbated and scaled up to the intensity of the Raman features. For this reason, the spectra gathered in cluster 5 (black) have been removed from the images and replaced by 0 in order to avoid interferences. The mean spectra corresponding to the different layers of the epidermis as clustered by the Kmeans clustering are presented in figure S2 in supplementary materials.

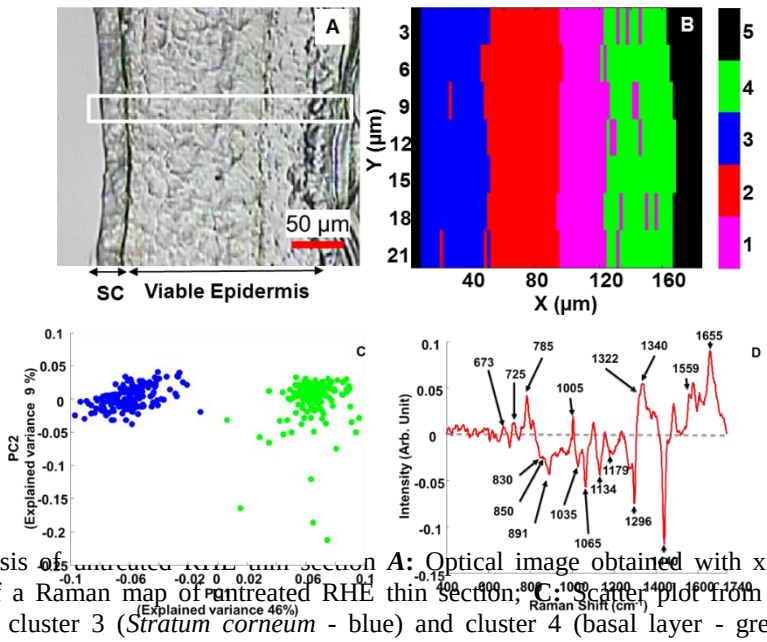

Figure 1 Raman analysis of untreated RHE thin section ***A:*** Optical image obtained with x50; **B:** K-means cluster analysis (5 clusters) of a Raman map of untreated RHE thin section; **C:** Scatter plot from the PCA performed on spectra extracted from cluster 3 (*Stratum corneum* - blue) and cluster 4 (basal layer - green); and **D:** Loading 1 corresponding to PC 1 of the PCA.

Despite the relevant histological information, K means clustering remains strongly limited to reflect biochemical variations in tissue sections, for instance in the human skin models, where differences are likely to be more concentration gradient like variations. The biochemical variations between the spectra corresponding to the different layers of the skin can be enhanced by means of PCA (Figure 1C). The scatter plot displays clear discrimination between the spectra extracted from cluster 3 (*Stratum corneum*) and cluster 4 (basal layer) of the K means clustering. The spectral signatures collected from skin section are highly complex and results from numerous combined contributions for the biochemical compounds shined under the laser, however the loading 1, shown in Figure 1D highlights the main spectral features involved in the data separation and thus reflects the modifications at the molecular level occurring during the cellular differentiation process. The major components of the *Stratum corneum* are the corneocytes, which are anuclear cells filled with keratin filaments and natural moisturizing factors (NMFs); corneodesmosomes (tight junctions between corneocytes); and an intercellular lipid bilayer matrix [45]. Their contributions can be observed at 1065 cm^{-1} and 1134 cm^{-1} representing the C-C stretching, 1296 cm^{-1} due to the CH_2 twisting and 1440 cm^{-1} due to CH_2 scissoring. The position of the amide I band at 1655 cm^{-1} reflects the increase in keratin in the human SC which adopts predominantly an α-helical conformation [46].

Cysteine, which is the major amino acid of keratin fibers [47] is characterized by Raman bands located at 673 cm^{-1} [48] supporting the presence of high amount of keratin in the SC. In contrast the basal layer is characterized by the proliferative activity of the keratinocytes constantly dividing. This is confirm by the apparition of features at 725 cm^{-1}, 1322 cm^{-1} and 1340 cm^{-1}, indicating the presence of both DNA and RNA, but also at 785 cm^{-1} which is more specific to DNA [48, 49]. Due to the maturation process taking place in the epidermis, it is not surprising to witness other spectral variations in the spectra collected from *Stratum corneum* and the basal layer. Most of these bands could be globally assigned to

changes in amino acids contents. For example, the features at 1005 cm^{-1} and 1035 cm^{-1} are commonly assigned to phenylalanine [48, 50] while tyrosine is rather identified with the doublet of Fermi between 830 cm^{-1} - 850 cm^{-1}. Another feature at 1559 cm^{-1} is assigned to tryptophan. All the wavenumbers highlighted by the PCA analysis reflect the important molecular dynamics taking place in the skin having a direct impact on the Raman signatures collected.

It also is interesting to perform a PCA analysis of the spectra extracted from cluster 3 (*stratum corneum*) obtained from Figure 1B, in order to highlight highly scattered spectra across the scatter plot along both PC1 and PC2 (Figure 2A), respectively accounting for 52% and 7% of the variance. The corresponding loadings have been plotted in Figure 2B_i and 2B_ii. As a comparison, spectra from albumin (Figure. 2B_iii), ceramide (Figure 2B_iv), and cholesterol (Figure 2B_v), which represent some of major features found in spectra collected from the *Stratum corneum*, have been also included. For example, the spectral features at 1677 cm^{-1}, 1340 cm^{-1}, 1005 cm^{-1}, 937 cm^{-1}, 850 cm^{-1} and 830 cm^{-1} correlate well with those found in proteins and the spectral features at 1440 cm^{-1}, 1296 cm^{-1} and 1065 cm^{-1} correlate with those found in lipids. Interpretation of the PCA suggests that using the K-means clustering analysis leads to a loss of information due to the rigid nature of the algorithm aiming to create well defined groups of spectra. It can be noticed that, inside the cluster, a degree of inter-variability can be expected directly linked to the quantitative information contained in the Raman spectra. Therefore, the spectral variation resulting from different amount of proteins or lipids between the data points assigned in a single cluster are not accessible. Naturally, the higher the number of clusters is, the lower would be the variability in each group formed, but it would not solve the problem of interpretation of the distribution of specific molecules according to their concentration and/or distribution. Further discussion and illustration of the limitation encountered with Kmeans clustering are provided in supplementary materials with figure S3.

The NCLS algorithm has been used in order to highlight the feasibility to overcome the limitation of grouping methods such as K means clustering. Although NCLS can be used to calculate residual spectra after subtraction of specific single Raman signatures from data sets, such as paraffin, [51] or contribution from substrate such as glass slides [34], it can also provide information about the abundance of multiple pure compounds. Basically, the method can use numerous reference spectra and combine them using adjusted coefficients in order to get an output spectrum as close as possible to the experimental spectrum. When applied to a Raman map, for each pixel, it is possible to calculate coefficients for each chemical component. Thus, it can produce a graphical representation of their distribution in a reconstructed false color map without losing the semi-quantitative information contained in the data sets. The same Raman map previously analysed using Kmeans clustering in Figure 1A has been subjected to NCLS using contributions of lipids, proteins and nucleic acids, as presented in Figure 3. The algorithm being based on the reference spectra input in the model, the contribution of each biomolecule in each Raman spectrum of the map, the task can be fastidious and covering all possibilities was not the aim of the study.

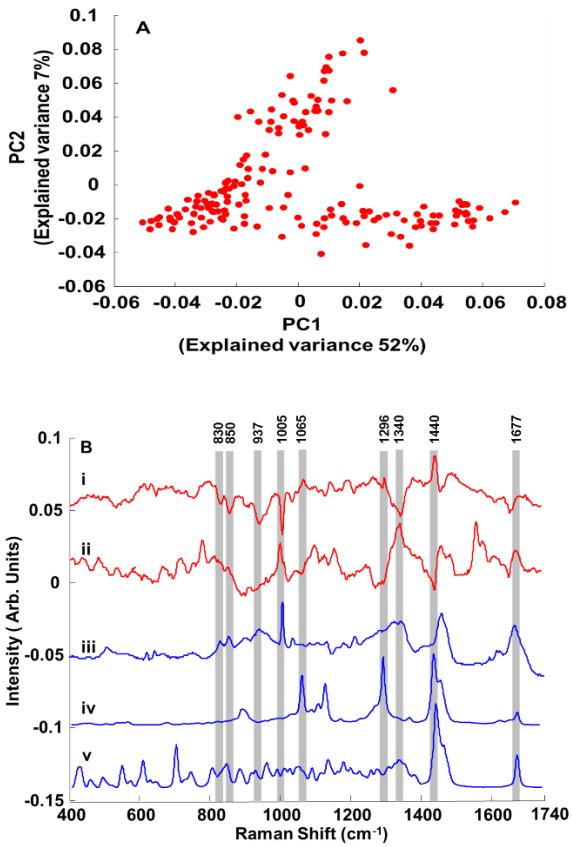

Figure 2 PCA performed on spectra corresponding to the *Stratum corneum* (Kmeans clustering - cluster 3) **A:** Scatter plot and **B:** Loading 1 (i) and loading 2 (ii) compared to pure spectrum of albumin (iii), ceramide (iv) and cholesterol (v).

As an example of such an analysis, a spectrum of ceramide has been selected to illustrate the contribution observed with lipid mostly found in the *stratum corneum* (Figure 3A). For comparison, a spectrum of histone representing the protein matrix (Figure 3B) and a spectrum from DNA representing the nucleic acids (Figure 3C) have also been included. The only commercially available keratin solutions are prepared

with urea; therefore, it is not possible to collect specific reference spectra from this protein. Therefore, histone has been preferred as an example of physiological compound found in the skin cells. For instance, the lipid matrix is well known as playing a key role in skin barrier function and has therefore been largely studied by means of Raman spectroscopy [52, 53]. Ceramides are synthetized in the latter stages of the skin maturation and consequently their contribution to the Raman spectra is located in the outer layers. The colour bars of the heat maps reconstructed from the NCLS indicate the relative contribution of the compound of interest in the RHE sections. The maximum of the colors has been arbitrarily fixed at 0.6 for consistency between the 3 examples presented in Figure 3. In the case of ceramide, between 0.1 (10%) and 0.2 (20%) was found in the *Stratum corneum* with no contribution observed in deepest layers such as the basal layer. In comparison, the proteins display higher levels of spectral contributions throughout the Raman map, having maximum at 0.6 (60%) observed in the basal layer while slightly decreasing to roughly 0.4 (40%) in the upper layers. Indeed, the protein matrix remains the main constituent of the skin even in the *Stratum corneum*, in which lipids have important functions in the barrier function. Interpretation of the protein heat map is more difficult compared to that of ceramide due to the presence of higher contents at the edge of the *Stratum corneum* and *Stratum granulosum*. This can be explained by the lack of keratin spectra as reference to compensate the spectral variations occurring in the most superficial layers and consequently a lack of specificity in the fitting. However, histones are present in the nucleolus of skin cells and it is therefore not surprising to observe the highest concentrations in the basal layer. Finally, the nucleic acids are mostly found in the basal layer, in which the keratinocytes have strong proliferative activities. Moreover, the DNA spectrum has been used in the model, further influencing the detection of cells with nuclear organelles which correlates with the rapid loss of nucleus in the differentiation process found in the skin. Ultimately, the NCLS allows to construct distribution maps of selected chemicals based on the specific information contained in the Raman spectra. The observations made of physiological biomolecules is encouraging, considering the small numbers of reference molecules input in the models. Indeed, the sensitivity of the analysis could be further increased using larger spectral banks to better fit the Raman signals, yet the results obtained from ceramide and DNA perfectly illustrate the potential and capabilities of the approach to detect and track some given substances in a complex biological matrix such as the skin.

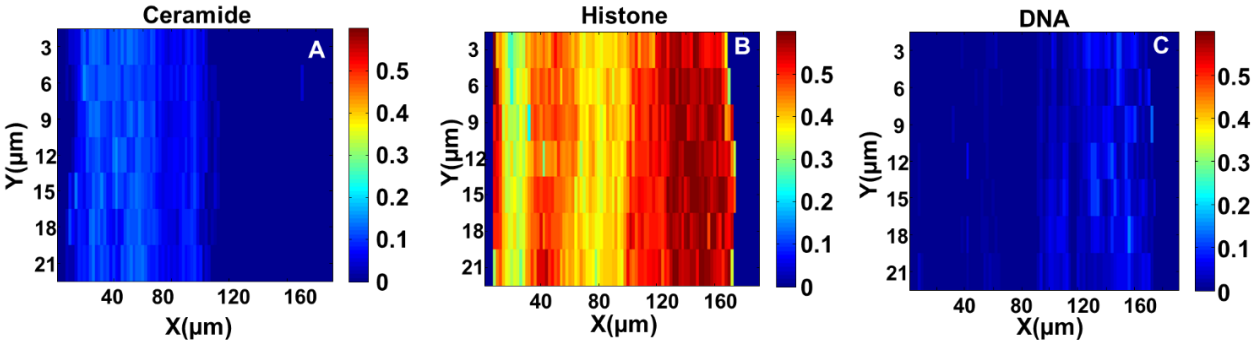

Figure 3 Reconstructed heat maps following NCLS analysis of control skin sections. **A:** Ceramide, **B:** Histone and **C:** DNA. Scale bar represent contribution of compound in the Raman spectra at each pixel. Maximum arbitrarily defined at 0.6 (60%) for consistency between 3 examples displayed.

3.2 Detection and tracking of an ACI in skin sections: The case of Delipidol®

The chemical structure of the Delipidol® used in this study is displayed in Figure 4A, with the corresponding vibrational modes assignments listed in table S1. The most intense features, observed at 1625 cm^{-1} (C=C stretching of the aromatic ring) and 1248 cm^{-1} (C-C-C stretching), clearly dominate the spectral signature (Figure 4C), leading to substantial modification in the spectra collected from the skin sections, as illustrated by the point spectrum from a sample exposed for 3 hours (Figure 4A and B). Other features at 1655 cm^{-1}, 1438 cm^{-1}, 1389 cm^{-1}, 1302 cm^{-1},1251cm^{-1}, 1206 cm^{-1}, 1160 cm^{-1}, 1073 cm^{-1}, 989 cm^{-1}, 968cm^{-1}, 863 cm^{-1}, 841 cm^{-1}, 824 cm^{-1}, and 642 cm^{-1} are hardly distinguishable in the plot by eye, due to lower intensities and the presence of numerous bands in the biological spectrum but they still contribute to the spectra recorded.

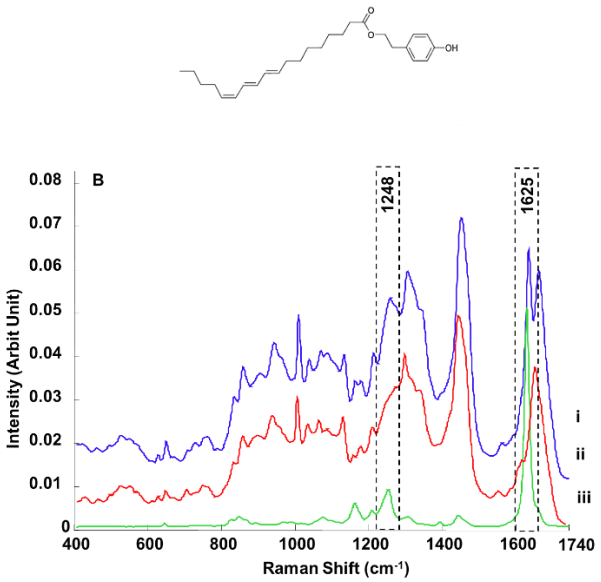

Figure 4 A: Chemical structure of the Delipidol®, **B:** Comparison between a typical Raman spectrum of the skin (i), a Raman spectrum of the skin following application of Delipidol® (ii) and the reference spectrum of Delipidol® (iii). Spectra are offset for clarity.

Working with an ACI implies that the molecular target is known prior to the start of the experiment and collection of reference spectra can be achieved for use in the NCLS analysis. However, the problem of false positives can arise during the analysis, if the reference spectra are not suitable as illustrated in Figure 5, in which an unexposed skin tissue section has been analysed. As seen in Figure 5A using only the Delipidol® spectrum leads to non-specific detection of the molecule throughout the spectral map collected from the control sample. Therefore, the presence of other reference spectra to counter balance the algorithm is necessary to ensure none of the ACI would be found in the control samples. An alternative that can be considered is the creation of Raman spectral banks for pre-defined reference compounds of interest representing the main skin constituents [54]. Figure 5B has been obtained using spectra from Delipidol®, ceramides, cholesterol, phosphatidylcholine, steric acid, histone, albumin and DNA. Although the outcome is improved compared to first attempt, some residual contribution of Delipidol® can still be observed in some areas of the skin section. Notably, in the area of the basal layer, some pixels exhibit up to about 0.05 (5%) Delipidol® contribution. The main difficulties encountered were, firstly the expense of the pure chemicals, considering just a few Raman spectra are required, and secondly acquisition of appropriate spectra as input to the model. Many of the reference materials can be purchased in different forms (powder, liquid), not necessarily delivering comparable signatures in terms of background and band ratios. Consequently, it is difficult to create a set of spectra matching perfectly with the data sets recorded from skin sections. In order to improve the specificity of the analysis, a third option has been explored, consisting of using all the spectra contained in a different control image (collected from a different skin section) as reference matrix for the NCLS analysis. For instance, the example illustrated in Figure 5C is obtained using a second Raman control map containing about 3000 spectra. It can be seen that no contribution of Delipidol® can be observed and that no false positive is obtained. Using large numbers of control spectra from independent Raman maps enables to take into account all variations in protein, lipids and nucleic acids in the different layers of the skin to produce an accurate fitting. Thus, this approach has been found more relevant for subsequent analysis.

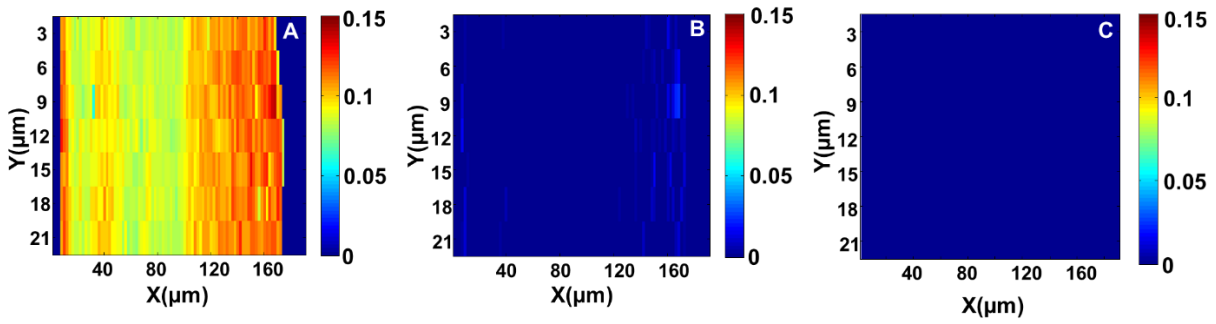

Figure 5 Reconstructed heat maps following NCLS analysis of control skin sections. **A:** Delipidol®, **B:** Delipidol®, ceramides, cholesterol, phosphatidylcholine, steric acid, histone, albumin and DNA, and **C:** Independent control spectra (about 3000). Scale bar represent the contribution of Delipidol® in the Raman spectra at each pixel. Maximum arbitrarily defined at 0.16 (16%) for consistency between 3 examples displayed.

Using the previous optimisation performed on a control skin section, Delipidol® distribution can be monitored after different incubation times (1h, 2h and 3h) in order to evaluate the penetration of the ACI. The results presented in Figure 6 highlight that, following 1h exposure time, the presence of Delipidol® is restricted to the *Stratum corneum*, indicating limited diffusion (Figure 6A). However, heat maps corresponding to 2h and 3h (respectively Figure 6B and 6C) illustrate increased penetration for longer exposure times, with initially higher contribution of the Delipidol® features in the *Stratum corneum*, followed by a diffusion into the deepest layers after 3h. As comparison, chemical maps of the Delipidol® distribution using its most intense feature at 1625 cm^{-1} are presented in figure 6 E-F-G for respectively 1H, 2H and 3H exposure times. Although the accumulation of the ACI in the *stratum corneum* can be also observed with single wavenumber reconstructed images, the information is not directly interpretable. The color bars provided only indicates relative intensities of the spectral band selected as seen in preprocessed spectra with contribution from underlying bands not considered. The maps corresponding to 1H exposure time perfectly illustrates the limitation of univariate approach. While the NCLS doesn't exhibit any contribution in the basal layer, the single band map would suggest the Delipidol® is found everywhere even for short exposure times. This is due to the partial overlap with the amide I band resulting in residual intensities in the maps. However, the NCLS is taking the contribution of other physiological compounds into account, simulated by means of references spectra, ultimately providing a better representation of the Delipidol® distribution. For better visualization of the relative concentration of the Delipidol® in the RHE, depth profiles can be established using the contribution coefficients calculated with the NCLS (Figure 7). The concentration profile is approximately single exponential for all three time points, with a consistent decay constant, which is independent of the sublayer structure. Working on reconstructed skin provides high intra- and inter- sample reproducibility by minimizing the variations in *Stratum corneum* thickness between anatomical sites and from person to person generally observed with *ex vivo* measurements. Thus, based on observations made using K-means clustering analysis, the delimitation between the *Stratum corneum* and the epidermis has been placed at about 40 µm. It can be seen that, for short exposure time (1h), the surface level of about 0.16 (16%) decays exponentially with depth, with the result that most of the ACI is located in the first 10 µm of the skin. For 2h exposure, the relative contribution at the surface has increased to 0.35 (35%), and a similar exponential decay with depth is observed. The levels of Delipidol® rapidly decrease and at about 30 µm depth no more contribution is found, supporting the notion that the *Stratum corneum* is not fully permeated. After 3h hours exposure time, although the surface levels continue to increase to ~0.6 (60%), and they decay with a similar profile, an approximately constant level of 0.11-0.2 (11%-20%) is observed between 30 µm and 100 µm. In terms of kinetics, it seems the concentration of Delipidol® gradually builds up in the *Stratum corneum*, to a point where no more can be accumulated, leading to leakage of the ACI in the subjacent skin layers. The exponential decay of the

Delipidol® profile across the *stratum corneum* is a result of the barrier function of the lipid rich layer to the ACI, which is explained by the presence of long alkyl chain conferring hydrophobicity to the molecule (Figure 5A). This retards the diffusion of the ACI into the epidermis over the first two hours of exposure. However, after 3-hour exposure, significant concentrations have diffused to the interface with the epidermal layer, at which point a relatively free diffusion results in accumulation of significant levels across the epidermis, which it the target region of interest (See 30 µm to 90 µm – Figure.7). Using Confocal Raman Spectroscopic Imaging, the kinetics of Delipidol® diffusion can be studied in order to better understand the molecule behavior in the skin layers. Ultimately, it highlights the difficulties of product design, by which an ACI or API should exhibit a good balance between hydrophobicity to breach the *Stratum corneum* and also hydrophilicity in order to be able to diffuse at sufficient concentrations in the deepest layers of the skin to have a substantial effect on the cellular targets. Spectral Raman imaging is therefore an ideal tool to screen and monitor newly identified candidates for cosmetic and pharmaceutical applications towards

dermal administration, but also to guide and support the recent

advancements in formation [1]. As proof of concept, the Delipidol® has been topically applied as an ethanol solution thus conferring an increased penetration due to enhancing effect of the solvent. However, the molecular specificity of the analysis would enable to perform comparative studies between different formulations such as gels or creams, with similar sensitivities. Notably, nowadays different encapsulating protocols are being optimized with the aim of enhancing ACI and API penetration through the *Stratum corneum* in order to increase the concentrations in the epidermis [55]. Developing efficient and specific multivariate methods will support the transfer of Confocal Raman Spectroscopic Imaging as reference technique in industrial routines. Moreover, the NCLS method described is adaptable to any data spectral data sets where only the references spectra need to be carefully selected to ensure maximum sensitivity. However, as much experimentations conducted in the cosmetic fields involve one or more control samples, the creation of suitable spectra bank for the NCLS is early not an obstacle.

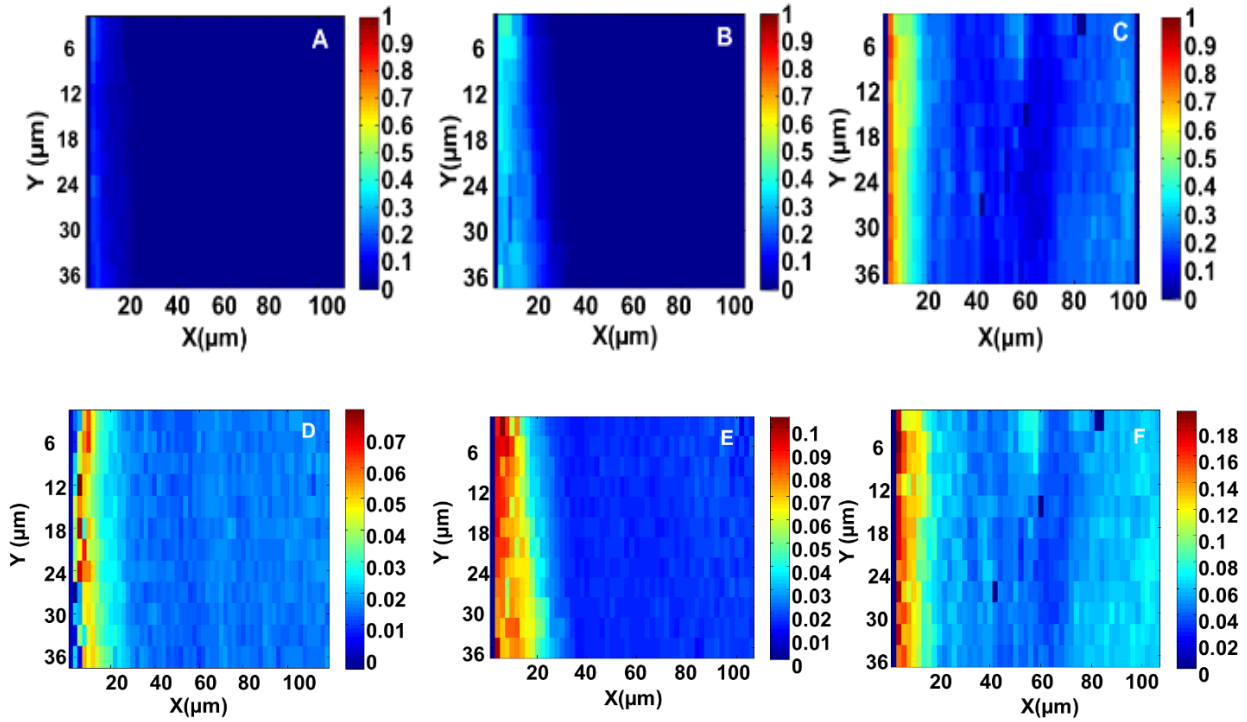

Figure 6 Reconstructed NCLS maps following NCLS analysis of skin samples exposed to Delipidol®. **A:** 1h, **B:** 2h and **C:** 3h; the scale bar represent the contribution of Delipidol® spectrum in the Raman spectra at each pixel compared with reconstructed maps obtained following univariate analysis of Delipidol® feature at 1625 cm^{-1} (D: 1h, E: 2h, F: 3h); the scale bar represent its relative intensity in preprocessed spectra.

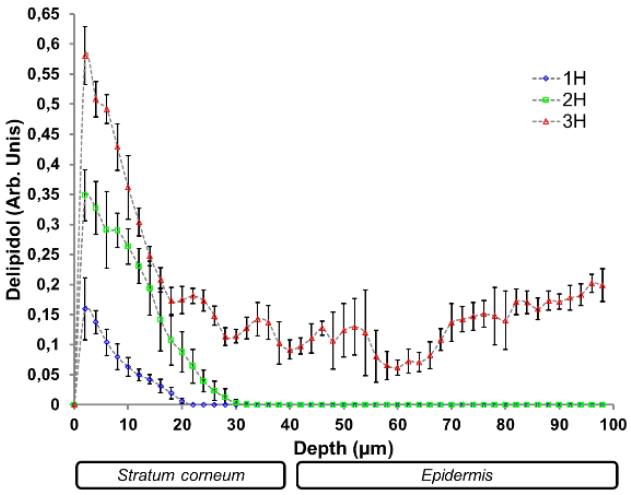

Figure 7 Penetration profiles of the Delipidol® obtained from the NCLS analysis following 1h (blue), 2h (green) and 3h (red) exposure times. The error bars are standard deviation calculated from the different lines of the Raman maps.

4. Conclusion

The specificity of the molecular information contained in the Raman spectra opens numerous perspectives for applications beyond fundamental research. For instance, Confocal Raman Spectroscopic Imaging is a powerful tool to support the constantly expanding field of skin administration of active ingredients. Given the extremely rapid turnover of relevant active molecules and formulation protocol for new cosmetic and pharmaceutical products, the technical repertoire available needs to deliver appropriate results for easy and reliable interpretations by users and customers. While K-means clustering analysis remains a valuable approach for analysis of Raman images collected from tissue sections providing histological information, more suitable methods need to be explored and validated to better answer to industrial requirements. Spectral unmixing methods such as NCLS enable to estimate the concentrations (by mean or abundance fractions) of known spectral signatures. Applied to the case of Delipidol®, chemical maps representing the ACI distribution throughout the skin section can be constructed. While the colour coded heat map represents the overall distribution reflecting the homogeneity of

diffusion of Delipidol® in the different skin layers, extraction of the abundance coefficient allows further exploitation of the quantitative information contained in the Raman spectra. Ultimately, analysis of the specific spectral features can elucidate the kinetics of ACI penetration in the skin using penetration profiles. The strive towards *in vitro* skin models for testing new ingredients or formulations, but also capabilities of Confocal Raman Imaging to detect and track molecules in a label free fashion without requiring substitution by fluorescent markers, clearly position the technique as highly relevant as a routine screening tool. Ultimately, optimization of data mining procedures towards automated protocols delivering accurate testing of ACI efficiency of penetration would further support the recognition of Confocal Raman spectroscopic Imaging for implementation in industrial environment.

Acknowledgements This work is part of the COSMICC project (2015-00103497). We thank Conseil Régional Centre Val de Loire and the ARD-2020 Cosmetosciences program for financial support.

Author biographies Please see Supporting Information online.

References

1. Nguyen HTP, Munnier E, Souce M, Perse X, David S, Bonnier F, Vial F, Yvergnaux F, Perrier T, Cohen-Jonathan S, Chourpa I, (2015) Novel alginate-based nanocarriers as a strategy to include high concentrations of hydrophobic compounds in hydrogels for topical application. Nanotechnology 26:255101. doi: 10.1088/0957-4484/26/25/255101

2. Rawlings A V., Matts PJ (2005) Stratum Corneum Moisturization at the Molecular Level: An Update in Relation to the Dry Skin Cycle. J Invest Dermatol 124:1099–1110. doi: 10.1111/j.1523-1747.2005.23726.x

3. Brown TJ, Alcorn D, Fraser JRE (1999) Absorption of Hyaluronan Applied to the Surface of Intact Skin. J Invest Dermatol 113:740–746. doi: 10.1046/j.1523-1747.1999.00745.x

4. HOFLAND HEJ, BOUWSTRA JA, BODDÉ HE, SPIES F, JUNGINGER HE (2010) Interactions between liposomes and human stratum corneum in vitro: freeze fracture electron microscopical visualization and small angle X-ray scattering studies. Br J Dermatol 132:853–866. doi: 10.1111/j.1365-2133.1995.tb16940.x

5. Bouwstra JA, de Vries MA, Gooris GS, Bras W, Brussee J, Ponec M (1991) Thermodynamic and structural aspects of the skin barrier. J Control Release 15:209–219. doi: 10.1016/0168-3659(91)90112-Q

6. Grams YY, Whitehead L, Cornwell P, Bouwstra JA (2004) On-Line Visualization of Dye Diffusion in Fresh Unfixed Human Skin. Pharm Res 21:851–859. doi: 10.1023/B:PHAM.0000026439.63969.30

7. Veiro JA, Cummins PG (1994) Imaging of Skin Epidermis from Various Origins Using Confocal Laser Scanning Microscopy. Dermatology 189:16–22. doi: 10.1159/000246752

8. Yu B, Langer R, Blankschtein D, Kim KH, So PTC (2003) Visualization of Oleic Acid-induced Transdermal Diffusion Pathways Using Two-photon Fluorescence Microscopy. J Invest Dermatol 120:448–455. doi: 10.1046/j.1523-1747.2003.12061.x

9. Krafft C, Popp J (2015) The many facets of Raman spectroscopy for biomedical analysis. Anal Bioanal Chem 407:699–717. doi: 10.1007/s00216-014-8311-9

10. Tfaili S, Gobinet C, Josse G, Angiboust J-F, Baillet A, Manfait M, Piot O (2013) Vibrational spectroscopies for the analysis of cutaneous permeation: experimental limiting factors identified in the case of caffeine penetration. Anal Bioanal Chem 405:1325–1332. doi: 10.1007/s00216-012-6512-7

11. Ali SM, Bonnier F, Ptasinski K, Lambkin H, Flynn K, Lyng FM, Byrne HJ (2013) Raman spectroscopic mapping for the analysis of solar radiation induced skin damage. Analyst 138:3946–3956. doi: 10.1039/c3an36617k

12. Butler H, Ashton L, Bird B, Cinque G, Curtis K (2016) Using Raman spectroscopy to characterize biological materials. Nat. Protoc.

13. Franzen L (2015) Applications of Raman spectroscopy in skin research — From skin physiology and diagnosis up to risk assessment and dermal drug delivery. Adv Drug Deliv Rev 89:91–104. doi: 10.1016/j.addr.2015.04.002

14. Vyumvuhore R, Tfayli A, Biniek K, Duplan H, Delalleau A, Manfait M, Dauskardt R, Baillet-Guffroy A (2015) The relationship between water loss, mechanical stress, and molecular structure of human *stratum corneum ex vivo*. J Biophotonics 8:217–225. doi: 10.1002/jbio.201300169

15. Chrit L, Bastien P, Biatry B, Simonnet J-T, Potter A, Minondo AM, Flament F, Bazin R, Sockalingum GD, Leroy F, Manfait M, Hadjur C (2007) In vitro and in vivo confocal Raman study of human skin hydration: Assessment of a new moisturizing agent,pMPC. Biopolymers 85:359–369. doi: 10.1002/bip.20644

16. Förster M, Bolzinger M, Ach D, Montagnac G (2011) Ingredients tracking of cosmetic formulations in the skin: a confocal Raman microscopy investigation. Pharmaceutical

17. Fleischli FD, Mathes S, Adlhart C (2013) Label free non-invasive imaging of topically applied actives in reconstructed human epidermis by confocal Raman spectroscopy. Vib Spectrosc 68:29–33. doi: 10.1016/j.vibspec.2013.05.003

18. Zhang G, Flach CR, Mendelsohn R (2007) Tracking the dephosphorylation of resveratrol triphosphate in skin by confocal Raman microscopy. J Control Release 123:141–147. doi: 10.1016/j.jconrel.2007.08.001

19. Tfaili S, Josse G, Angiboust JF, Manfait M, Piot O (2014) Monitoring caffeine and resveratrol cutaneous permeation by confocal Raman microspectroscopy. J Biophotonics. doi: 10.1002/jbio.201300011

20. Essendoubi M, Gobinet C, Reynaud R, Angiboust JF, Manfait M, Piot O (2016) Human skin penetration of hyaluronic acid of different molecular weights as probed by Raman spectroscopy. Ski Res Technol 22:55–62. doi: 10.1111/srt.12228

21. Pyatski Y, Zhang Q, Mendelsohn R, Flach C (2016) Effects of permeation enhancers on flufenamic acid delivery in Ex vivo human skin by confocal Raman microscopy. Int. J.

22. Links DA (2012) Understanding the molecular information contained in principal component analysis of vibrational spectra of biological systems. 322–332. doi: 10.1039/c1an15821j

23. Bonnier F, Knief P, Lim B, Meade AD, Dorney J, Bhattacharya K, Lyng FM, Byrne HJ, Roddy P, Hannun YA, Chalfant CE (2010) Imaging live cells grown on a three dimensional collagen matrix using Raman microspectroscopy. Analyst 135:3169. doi: 10.1039/c0an00539h

24. Ly E, Piot O, Wolthuis R, Durlach A, Bernard P, Manfait M (2008) Combination of FTIRspectral imaging and chemometrics for tumour detection from paraffin-embedded biopsies. Analyst 133:197–205. doi: 10.1039/B715924B

25. Tfayli A, Piot O, Pitre F, Manfait M (2007) Follow-up of drug permeation through excised human skin with confocal Raman microspectroscopy. Eur Biophys J 36:1049–1058. doi: 10.1007/s00249-007-0191-x

26. Netzlaff F, Lehr C-M, Wertz PW, Schaefer UF The human epidermis models EpiSkin w , SkinEthic w and EpiDerm w : An evaluation of morphology and their suitability for testing phototoxicity , irritancy , corrosivity , and substance transport. doi: 10.1016/j.ejpb.2005.03.004

27. Ponec M, Boelsma E, Gibbs S, Mommaas M (2002) Characterization of reconstructed skin models. Skin Pharmacol Appl Skin Physiol 15 Suppl 1:4–17. doi: 66682

28. Netzlaff F, Kaca M, Bock U, Haltner-Ukomadu E, Meiers P, Lehr C-M, Schaefer UF (2007) Permeability of the reconstructed human epidermis model Episkin® in comparison to various human skin preparations. Eur J Pharm Biopharm 66:127–134. doi: 10.1016/j.ejpb.2006.08.012

29. Tfayli A, Piot O, Manfait M (2008) Confocal Raman microspectroscopy on excised human skin: uncertainties in depth profiling and mathematical correction applied to dermatological drug permeation. J Biophotonics 1:140–153. doi: 10.1002/jbio.200710004

30. Tfayli A, Gobinet C, Vrabie V, Huez R, Manfait M, Piot O (2009) Digital Dewaxing of Raman Signals: Discrimination Between Nevi and Melanoma Spectra Obtained from Paraffin-Embedded Skin Biopsies. Appl Spectrosc Vol 63, Issue 5, pp 564-570 63:564–570.

31. Farhane Z, Bonnier F, Maher MA, Bryant J, Casey A, Byrne HJ (2017) Differentiating responses of lung cancer cell lines to Doxorubicin exposure: *in vitro* Raman micro

spectroscopy, oxidative stress and bcl-2 protein expression. J Biophotonics 10:151–165. doi: 10.1002/jbio.201600019

32. Kwan C, Ayhan B, Chen G, Jing Wang, Baohong Ji, Chein-I Chang (2006) A novel approach for spectral unmixing, classification, and concentration estimation of chemical and biological agents. IEEE Trans Geosci Remote Sens 44:409–419. doi: 10.1109/TGRS.2005.860985

33. Netzlaff F, Lehr C-M, Wertz PW, Schaefer UF The human epidermis models EpiSkin w , SkinEthic w and EpiDerm w : An evaluation of morphology and their suitability for testing phototoxicity , irritancy , corrosivity , and substance transport. doi: 10.1016/j.ejpb.2005.03.004

34. Byrne HJ, Knief P, Keating ME, Bonnier F (2016) Spectral pre and post processing for infrared and Raman spectroscopy of biological tissues and cells. Chem Soc Rev. doi: 10.1039/C5CS00440C

35. Hedegaard M, Krafft C, Ditzel HJ, Johansen LE, Hassing S, Popp J (2010) Discriminating Isogenic Cancer Cells and Identifying Altered Unsaturated Fatty Acid Content as Associated with Metastasis Status, Using K-Means Clustering and Partial Least Squares-Discriminant Analysis of Raman Maps. Anal Chem 82:2797–2802. doi: 10.1021/ac902717d

36. Bonnier F, Knief P, Lim B, Meade AD, Dorney J, Bhattacharya K, Lyng FM, Byrne HJ (2010) Imaging live cells grown on a three dimensional collagen matrix using Raman microspectroscopy. Analyst 135:3169. doi: 10.1039/c0an00539h

37. Bonnier F, Byrne HJ, Juhola M (2012) Understanding the molecular information contained in principal component analysis of vibrational spectra of biological systems. Analyst 137:322–332. doi: 10.1039/C1AN15821J

38. Bonnier F, Byrne HJ (2012) Understanding the molecular information contained in principal component analysis of vibrational spectra of biological systems. Analyst 137:322. doi: 10.1039/c1an15821j

39. Kwan C, Ayhan B, Chen G, Wang J, Ji B, Chang C-I (2006) A Novel Approach for Spectral Unmixing , Classification , and Concentration Estimation of Chemical and Biological Agents. IEEE Trans Geosci Remote Sens. doi: 10.1109/TGRS.2005.860985

40. Gobinet C, Sebiskveradze D, Vrabie V, Tfayli A, Piot O, Manfait M DIGITAL DEWAXING OF RAMAN SPECTRAL IMAGES OF PARAFFIN-EMBEDDED HUMAN SKIN BIOPSIES BASED ON ICA AND NCLS.

41. Miloudi L, Bonnier F, Bertrand D, Byrne HJ, Perse X, Chourpa I, Munnier E (2017) Quantitative analysis of curcumin-loaded alginate nanocarriers in hydrogels using Raman and attenuated total reflection infrared spectroscopy. Anal Bioanal Chem 409:4593–4605. doi: 10.1007/s00216-017-0402-y

42. Bonnier F, Ali SM, Knief P, Lambkin H, Flynn K, McDonagh V, Healy C, Lee TC, Lyng FM, Byrne HJ (2012) Analysis of human skin tissue by Raman microspectroscopy: Dealing with the background. Vib Spectrosc. doi: 10.1016/j.vibspec.2012.03.009

43. Rashid N, Nawaz H, Poon KWC, Bonnier F, Bakhiet S, Martin C, O'Leary JJ, Byrne HJ, Lyng FM (2014) Raman microspectroscopy for the early detection of pre-malignant changes in cervical tissue. Exp Mol Pathol 97:554–64. doi: 10.1016/j.yexmp.2014.10.013

44. Koljenovi? S, Choo-Smith L-P, Bakker Schut TC, Kros JM, van den Berge HJ, Puppels GJ (2002) Discriminating Vital Tumor from Necrotic Tissue in Human Glioblastoma Tissue Samples by Raman Spectroscopy. Lab Investig 82:1265–1277. doi: 10.1097/01.LAB.0000032545.96931.B8

45. Vyumvuhore R, Tfayli A, Duplan H, Delalleau A, Manfait M, Baillet-Guffroy A (2013) Effects of atmospheric relative humidity on Stratum Corneum structure at the molecular level: ex vivo Raman spectroscopy analysis. Analyst 138:4103. doi: 10.1039/c3an00716b

46. Ali SM, Bonnier F, Tfayli A, Lambkin H, Flynn K, McDonagh V, Healy C, Clive Lee T, Lyng FM, Byrne HJ (2012) Raman spectroscopic analysis of human skin tissue sections *ex-vivo* : evaluation of the effects of tissue processing and dewaxing. J Biomed Opt 18:61202. doi: 10.1117/1.JBO.18.6.061202

47. Baden HP, Bonar L, Katz E (1968) Fibrous Proteins of Epidermis**From the Departments of Dermatology and Orthopedic Research of the

Harvard Medical School and the Massachusetts General Hospital, Boston, Massachusetts 02114. J Invest Dermatol 50:301–307. doi: 10.1038/jid.1968.48

48. Tfayli A, Piot O, Draux F, Pitre F, Manfait M (2007) Molecular Characterization of Reconstructed Skin Model by Raman Microspectroscopy : Comparison with Excised Human Skin. doi: 10.1002/bip.20832

49. Ali SM, Bonnier F, Lambkin H, Flynn K, McDonagh V, Healy C, Lee TC, Lyng FM, Byrne HJ, Draux F, Jeannesson P, Beljebbar A, Tfayli A, Fourre N, Manfait M, Sule-Suso J, Sockalingum GD, (2013) A comparison of Raman, FTIR and ATR-FTIR micro spectroscopy for imaging human skin tissue sections. Anal Methods 5:2281. doi: 10.1039/c3ay40185e

50. Stone N, Kendall C, Smith J, Crow P, Barr H (2004) Raman spectroscopy for identification of epithelial cancers. Faraday Discuss 126:141. doi: 10.1039/b304992b

51. Tfayli A, Gobinet C, Manfait M, Piot O, Huez R, Vrabie V (2009) Digital Dewaxing of Raman Signals: Discrimination Between Nevi and Melanoma Spectra Obtained from Paraffin-Embedded Skin Biopsies. Appl Spectrosc Vol 63, Issue 5, pp 564-570 63:564–570.

52. Vyumvuhore R, Tfayli A, Duplan H, Delalleau A, Manfait M, Baillet-Guffroy A (2013) Effects of atmospheric relative humidity on Stratum Corneum structure at the molecular level: ex vivo Raman spectroscopy analysis. Analyst 138:4103. doi: 10.1039/c3an00716b

53. Tfayli A, Guillard E, Manfait M, Baillet-Guffroy A (2012) Raman spectroscopy: feasibility of in vivo survey of stratum corneum lipids, effect of natural aging. Eur J Dermatol 22:36–41. doi: 10.1684/ejd.2011.1507

54. Keating ME, Bonnier F, Byrne HJ (2012) Spectral cross-correlation as a supervised approach for the analysis of complex Raman datasets: the case of nanoparticles in biological cells. Analyst 5792–5802. doi: 10.1039/c2an36169h

55. Nguyen HTP, Allard-Vannier E, Gaillard C, Eddaoudi I, Miloudi L, Soucé M, Chourpa I, Munnier E (2016) On the interaction of alginate-based core-shell nanocarriers with keratinocytes in vitro. Colloids Surfaces B Biointerfaces. doi: 10.1016/j.colsurfb.2016.02.055

Graphical Abstract for Table of Contents

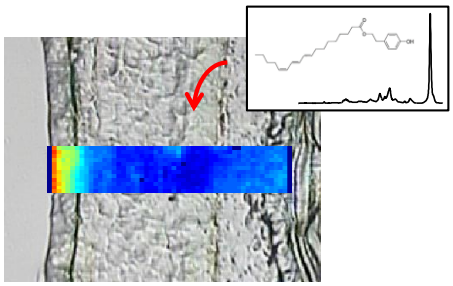

Text: label free tracking of active cosmetic ingredient in reconstructed human skin using the specific molecular signature of Raman spectra opens numerous perspectives for implementation as screening tool for industrial use